Evaluation of Lamina Cribrosa and Peripapillary Sclera Stiffness in Pseudoexfoliation and Normal Eyes by Atomic Force Microscopy

Christoph Braunsmann,[1,2] *Christian M. Hammer,*[2,3] *Johannes Rheinlaender,*[1] *Friedrich E. Kruse,*[3] *Tilman E. Schäffer,*[*,1] *and Ursula Schlötzer-Schrehardt*[*,3]

Purpose. Pseudoexfoliation (PEX) syndrome is a systemic disorder of the elastic fiber system that can lead to PEX glaucoma. Elastotic alterations in the lamina cribrosa (LC) of PEX eyes suggested biomechanical implications predisposing to pressure-induced optic nerve damage. In this pilot study, the stiffness of LC and peripapillary sclera (ppSC) in eyes with and without PEX syndrome were analyzed by atomic force microscopy (AFM) nanoindentation.

Methods. Unfixed cryosections (5-μm thick) were prepared from the optic nerve heads (ONH) of three donor eyes with PEX syndrome and three age-matched control eyes. AFM force mapping was performed in selected regions of the central, midperipheral, and peripheral LC and the ppSC using a spherical cantilever tip. To determine the local Young's modulus of elasticity (YME) as a measure of tissue stiffness, force curves were acquired and analyzed using the spherical Hertz model.

Results. For the LC, the median YME values calculated from single stiffness maps averaged 17.2 (±2.7) kPa in normal eyes and 10.1 (±1.4) kPa in PEX eyes, indicating a significant PEX-related decrease in stiffness by over 40% ($P < 0.01$). The corresponding YME values for the ppSC, which revealed a 9-fold higher tissue stiffness than in the LC, averaged 158.3 (±59.8) kPa for control and 85.8 (±16.9) kPa for PEX samples.

Conclusions. AFM was proven suitable for determining the stiffness of ONH tissues, encouraging further large-scale analyses. The marked decrease in stiffness, implying an increased deformability of the ONH in PEX eyes, may reflect an inherent tissue weakness rendering these eyes more vulnerable to glaucomatous damage. (*Invest Ophthalmol Vis Sci.* 2012;53:2960–2967) DOI:10.1167/iovs.11-8409

From the [1]Institute of Applied Physics, and the [3]Department of Ophthalmology, Friedrich-Alexander-University of Erlangen-Nürnberg, Erlangen, Germany.

[2]These authors contributed equally to this work and should therefore be regarded as equivalent authors.

Supported by NanoWorld and Asylum Research.

Submitted for publication August 12, 2011; revised January 2 and February 20, 2012; accepted March 16, 2012.

Disclosure: **C. Braunsmann**, None; **C.M. Hammer**, None; **J. Rheinlaender**, None; **F.E. Kruse**, None; **T.E. Schäffer**, None; **U. Schlötzer-Schrehardt**, None

*Each of the following is a corresponding author: Tilman E. Schäffer, Institute of Applied Physics, University of Tübingen, Auf der Morgenstelle 10, 72076 Tübingen, Germany; tilman.schaeffer@uni-tuebingen.de.

Ursula Schlötzer-Schrehardt, Department of Ophthalmology, University of Erlangen-Nürnberg, Schwabachanlage 6, 91054 Erlangen, Germany; ursula.schloetzer-schrehardt@uk-erlangen.de.

Pseudoexfoliation (PEX) syndrome is a genetically determined, age-dependent generalized disorder of the elastic fiber system.[1] It may affect up to 25% of the general population over 60 years of age worldwide and is characterized by an excessive production and aggregation of elastic microfibrils into abnormal PEX fibrils within a multitude of intra- and extraocular tissues.[1,2] Accumulation of this pathologic material in the aqueous humor outflow pathways predisposes to ocular hypertension and development of a severe type of open-angle glaucoma, known as PEX glaucoma.[3,4] Compared with other glaucomatous disorders, PEX glaucoma is typically associated with particularly high levels and pronounced diurnal fluctuations of intraocular pressure (IOP),[5,6] a high incidence of optic nerve damage,[7] and an exceptionally rapid progression.[8]

Among the factors contributing to poor prognosis and fast progression may be pronounced abnormalities of the elastic fiber system, which have been previously described in the lamina cribrosa (LC) of eyes with PEX glaucoma.[9,10] These studies demonstrated a marked and site-specific elastosis of the laminar beams in PEX glaucoma, which was significantly more pronounced than in other types of glaucoma. More recently, conspicuous elastotic alterations were also described in the LC of early stages of PEX syndrome without glaucoma,[11] suggesting a PEX-specific primary defect in elastin metabolism, which may adversely affect the biomechanical properties of the LC and render these eyes more vulnerable to IOP-induced optic nerve damage. However, the causal link between the morphologically evident elastosis and biomechanical alterations has not been established so far.

Atomic force microscopy (AFM)[12] has proven a powerful technology for high-resolution imaging of surface topography and for probing mechanical properties including Young's modulus of elasticity (YME) of biological samples.[13] In this pilot study, we evaluated the suitability of AFM nanoindentation-based force mapping for a direct measurement and comparative analysis of tissue stiffness in unfixed sections of LC and peripapillary sclera (ppSC) obtained from eyes with and without PEX syndrome. We herein present the first PEX-related stiffness data of the optic nerve head (ONH) region and show marked differences in YME between PEX and control specimens.

Methods

Sample Preparation

The ONHs of six grossly age-matched human donor eyes with ($n = 3$; 77, 84, and 92 years) and without ($n = 3$; 64, 72, and 88 years) PEX syndrome were prepared under a dissecting microscope, embedded in Tissue Tek O.C.T. Compound (Sakura Finetek Germany, Staufen, Germany), and shock-frozen in liquid nitrogen–cooled isopentane.

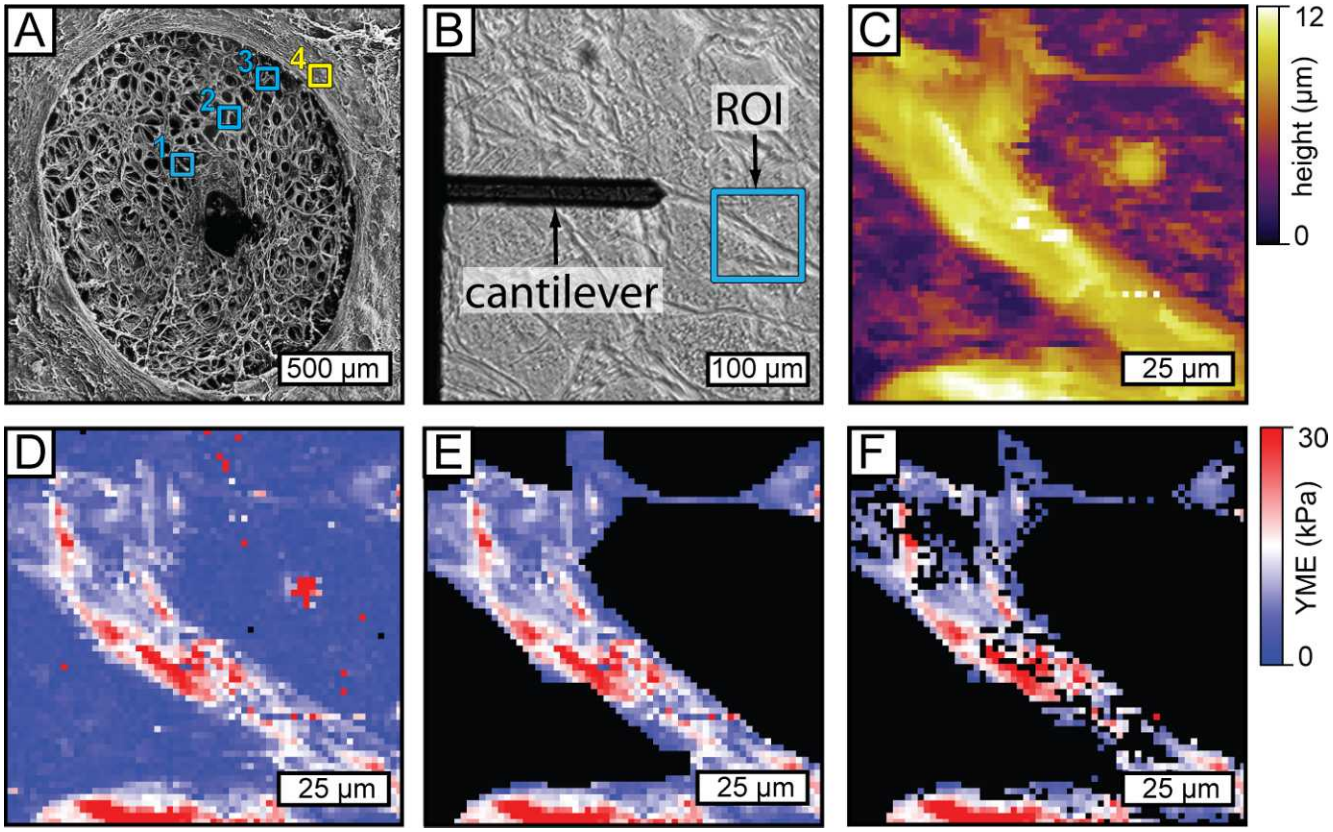

Figure 1. AFM force mapping procedure. (**A**) Scanning electron micrograph depicting measurement locations (Courtesy of CY Mardin, Erlangen, Germany). One laminar beam was evaluated in the (1) central, (2) midperipheral, and (3) peripheral region of the superior LC in each specimen. One reading was taken from (4) the ppSC. (**B**) ROI selection. Regions of interest (90×90 µm^2) were selected manually by using an inverted light microscope. Care was taken that every ROI contained at least one intact laminar beam or an intact area of peripapillary sclera. (**C**) Topography image. Force mapping trigger height image of the ROI shown in (**B**) (64×64 pixels, 50 nN trigger force, 20 µm/s force curve velocity). A laminar beam is clearly visible (*yellow*). (**D**) Stiffness image containing all data points. Every data point (*pixel*) represents one individual force curve and, hence, one local YME. (**E**) Stiffness image with irrelevant areas excluded. Irrelevant areas such as the laminar pores were determined by inspection of the topography image (**C**) and were demarcated by a black mask. These areas were excluded from analysis. (**F**) Stiffness image with exclusion of unsatisfactory Hertz fits. YMEs derived from Hertz fits with an average absolute deviation of >300 pm were considered of poor quality and were excluded from further analysis.

The presence of PEX was determined by macroscopically visible deposits of PEX material on anterior segment structures, such as the lens, iris, ciliary processes, and zonules, and confirmed by electron microscopic analysis of small tissue sectors.[1] The absence of glaucoma and other ocular diseases was confirmed by patients' histories obtained from the eye banks and by microscopic analysis of optic nerve cross-sections. Normal donor eyes had no history of eye disease and no macroscopic evidence of any pathology. Informed consent to tissue donation was obtained from the patients or their relatives, and the protocol of the study was approved by the local Ethics Committee and adhered to the tenets of the Declaration of Helsinki for experiments involving human tissues and samples.

ONH cross-sections of 5-µm thickness were prepared at the level of the LC using a Leica CM3050 cryostat (Leica GmbH, Bensheim, Germany). We note that samples for AFM must have a very low surface roughness to ensure an unobstructed tip–sample contact. Cryotoming provided sufficiently flat samples that could be investigated by AFM. For comparative analyses, we consistently used the first complete section through the anterior LC obtained by cutting serial cross-sections starting from the retinal surface. The unfixed cryosections were mounted on gelatin-coated glass slides, dried, and subsequently stored at −20°C overnight. Prior to AFM force mapping, the specimens were thawed, equilibrated to room temperature for approximately 30 minutes, and reconstituted in PBS to remove the embedding medium. Thorough removal of O.C.T. compound was confirmed by use of an inverted light microscope (TI-S, Nikon, Tokyo, Japan). Force maps were recorded in PBS.

Regions of Interest (ROIs)

The scanning electron micrograph shown in Figure 1A depicts an anterior view of a normal human LC and illustrates the ROIs selected for force mapping. In every specimen, one ROI was placed on the ppSC and three ROIs on connective tissue beams in central, midperipheral, and peripheral regions of the superior quadrant of the LC. After visual selection of a suitable ROI (Fig. 1B), the cantilever tip was positioned and force mapping was initiated.

AFM Force Mapping

AFM force-versus-distance curves (force curves) were generated to determine the local YME as a measure of tissue stiffness of LC and ppSC connective tissues. Force curve measurements were conducted as described elsewhere.[14–17] Briefly, z-displacement of the AFM scanner and AFM cantilever deflection were recorded while approaching the cantilever tip towards the sample. Force-versus-sample indentation behavior was evaluated to determine the contact point and the local YME of the sample. We applied the spherical Hertz model[18] that describes the sample indentation δ of a homogenous, elastic half-space by a spherical indenter with loading force F according toshow

$$F = \frac{4}{3}\frac{E\sqrt{R}\delta^{3/2}}{1-\nu^2}.$$

In this formula, E is the local YME, R is the radius of the spherical indenter, and ν is the Poisson's ratio, assumed as 0.5 for an incompressible sample. The sample indentation δ was determined as the difference between z-displacement z and deflection d relative to the contact point (z_0, d_0)

$$\delta = (z - z_0) - (d - d_0).$$

The YME was obtained by fitting the Hertz model to the data. In force-mapping mode,[19] 64 × 64 force curves were recorded on a 90-μm × 90-μm scan area. Hertz model analysis of all force curves resulted in a "stiffness image" of the scan area investigated. Mapping the z-positions z_{trig} at which the predefined maximum force of 50 nN (trigger force) was reached resulted in a topography image of the indented sample, termed "trigger height image." Force curve velocity was set to 20 μm/s.

All force-mapping experiments were performed with a MFP-3D-BIO atomic force microscope (Asylum Research, Santa Barbara, CA) combined with an inverted Ti-S light microscope to visually control sample and cantilever positions. The AFM was equipped with position sensors, thereby making the measured z-displacement and indentation independent of piezo nonlinearities.

Data Analysis

Figures 1B–F show an exemplary measurement procedure on a representative LC beam. In the trigger height image (Fig. 1C), the connective tissue beams could be readily identified and distinguished from the LC pores containing remains of optic nerve axons, which were excluded from further evaluation. This preselection was performed according to a mask obtained from the trigger height image (Fig. 1C). It should be noted that the trigger height image shows a height difference of up to 12 μm, although the cryosections were cut at a thickness of just 5 μm. An explanation for this large variation in height, which is found in both the PEX and normal eye samples, might be provided by different swelling characteristics for the LC beams and the remains of the optic nerve axons after rehydration. Furthermore, the LC pores probably were not densely filled with axons before cryotoming. It is known for other biological samples like chromosomes and collagen fibrils that rehydration can increase the sample volume by a factor of 4.0 to 5.5,[20,21] explaining the large height difference observed. A stiffness image representing the complete ROI area is given in Figure 1D; whereas in Figure 1E, areas excluded from further analysis are blackened according to the mask obtained above. The connective tissue areas exhibited clear local deviations in YME ranging from 3 kPa to approximately 30 kPa.

Hertz Model. The Hertz model describes the forced elastic indentation of a homogeneous, smooth sample of infinite thickness. Even if these requirements are not fulfilled, the Hertz model is still a good approximation, as long as (1) the sample is locally homogenous, (2) the sample roughness is small in comparison to the size of the tip, and (3) the indentation is small in comparison to the sample thickness. On top of the LC beams, for example, these requirements were mostly met. Here, only the spherical tip end touched the comparably smooth and homogenous sample surface during nanoindentation, and the recorded force curves could be clearly separated in a flat non-contact region and in a contact region where the force increased monotonously with increasing indentation. Consequently, the Hertz model fits matched the force curve data with adequate accuracy and thus yielded reliable stiffness values. At other positions, the tip-sample contact was less well defined. Directly adjacent to steep structures (e.g., at the rims of the LC beams), the sample surface was sometimes contacted by the cantilever beam instead of or in addition to the tip end. In other cases, the tip slipped off the beam sideways. On inhomogeneous, soft, and thin regions, such as the remains of the optic nerve axons, the tip sometimes penetrated the sample until it sensed the much stiffer substrate. For these non-Hertzian contacts, a clear separation into non-contact and contact regions was impossible. The force curve data did not follow a Hertzian indentation pathway, and thus the poorly matching Hertz model fits gave erroneous stiffness values, which could not be considered for data analysis. We therefore applied a "fit-quality criterion" to address this issue. The fit-quality can be expressed by the sum of the squared differences between the fitted Hertz model and the experimental data:

$$\chi \equiv \sum_j \left(\frac{\delta - \delta_j}{\sigma_j}\right)^2.$$

Here, δ represents the fitted indentation value for a given point, δ_j stands for the measured indentation at that point, and σ_j is a weighting value. We considered each data point to have the same accuracy and set $\sigma_j = 1$. In a computational least square fit, χ is minimized by iteratively improving the fitting parameters. The average absolute deviation of the experimental data from the model is given by $\varepsilon \equiv \sqrt{\chi}/N$, where N is the number of data points per force curve. The smaller the ε, the better the model fits the experimental data. For the force map shown in Figure 1, ε ranged from 0 to 1.5 nm. We excluded all YMEs obtained from force curves with $\varepsilon > 0.3$ nm to get more reliable results. Figure 1F shows the stiffness image after additional application of this fit-quality criterion.

It is apparent from Figure 1F that the stiffness of the LC beam still shows large local deviations (e.g., owing to differences in collagen and elastic fiber density and cross-linking). Therefore, it is necessary to record a high number of force curves to obtain sufficient statistics. Since high-resolution force maps already contain a large number of force curves (in our case 4096), force mapping is preferable to recording single force curves on spatially independent regions, especially on soft and inhomogeneous composite materials like LC and ppSC connective tissues. Moreover, force maps allow the collection of topography data in addition to stiffness information, which is necessary to distinguish between different tissue components.

Sphere Tip Cantilever

Spherical cantilever tips with a large radius ($R > 500$ nm) can be advantageous for the determination of characteristic mean YME values since they result in a large contact area, which compensates for local deviations of sample composition. The resulting small contact pressure, as compared with that from sharp tips ($R \approx 10$ nm), additionally reduces unwanted sample damage. Here, we used a sphere tip cantilever (Sphere Tips FM-M, NanoWorld, Neuchâtel, Switzerland) with a radius of 1 μm (Fig. 2A). As the tip apex was perfectly spherical, the use of the spherical Hertz model was justified. The use of relatively long cantilever tips (13–15 μm) was crucial to overcome the large differences in sample height of the sectioned ONH tissue specimens. A force constant of 4.5 nN/nm was determined by the thermal noise method.[22–24]

Utmost care was taken to maximize the repeatability of the experiments. Three main sources of error in AFM nanoindentation experiments are known, which all concern the cantilever: (1) the calibration of the cantilever spring constant, (2) tip shape or radius alterations, and (3) changes of the sensitivity of the optical beam deflection system. Since the same cantilever was used for all 24 force maps generated for this study (totaling more than 100,000 individual force curves), the systematic error of up to ≈20% in spring constant determination[25,26] did not affect the relative comparison of sample stiffness. Differences in tip shape due to the use of different cantilevers are meaningless for the same reason. To reduce tip shape alterations caused by organic contaminations, we removed the cantilever from the AFM in between each of the 24 force maps, rinsed it with distilled water and ethanol, dried it with nitrogen, and then removed potentially remaining organic residues by UV ozone cleaning. Figures 2B and 2C show a scanning electron microscopy (SEM) image of the spherical apex before and after the force map measurements, respectively. SEM evaluation of the cantilever tip after completion of all force-map

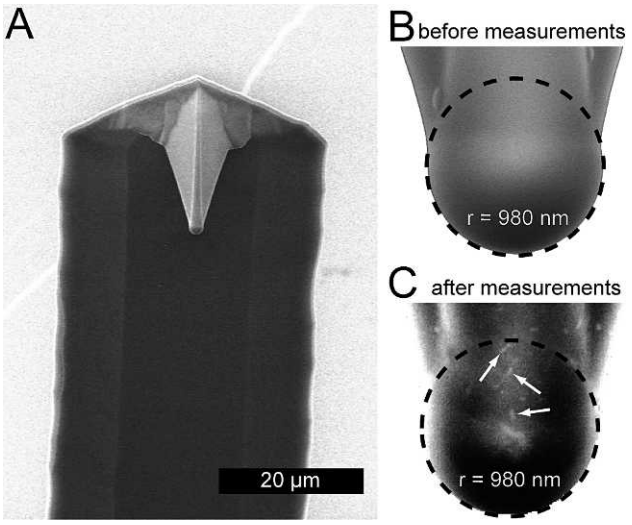

Figure 2. Scanning electron micrograph of the sphere tip cantilever used in this study (NanoWorld Sphere Tips FM-M). (**A**) Cantilever with tip. In the course of this study, approximately 100,000 force curves were generated with the cantilever shown here. (**B**) Sphere tip before measurements. The radius of the spherical tip apex was 980 nm (*dashed circle*). (**C**) Sphere tip after measurements. Shape and radius of the tip apex remained unaltered and showed no signs of wear.

measurements yielded a radius of 980 nm and showed no detectable alterations as a result of tip wear. The minute organic residues found (Fig. 2C, white arrows) were considered too small to cause any disturbance of the interactions between tip and sample. The optical beam deflection system measuring the cantilever deflection was calibrated before each force map by a force curve on the stiff glass slide adjacent to the ONH cryosections.

To confirm the repeatability of AFM force mapping, three consecutive measurements were performed over the same area of normal LC cryosections with complete removal of the tip in between the force maps. Supplementary Figure S1 shows an example of three repetitive stiffness maps obtained from one LC beam (see Supplementary material and Supplementary Fig. S1, http://www.iovs.org/lookup/suppl/doi:10.1167/iovs.11-8409/-/DCSupplemental). The median stiffness varied by less than 6%. This variation was statistically not significant with respect to the interquartile ranges, confirming repeatability of measurements.

Results

Figure 3 shows representative examples of topography and stiffness images obtained from the LC (Figs. 3A–D) and ppSC (Figs. 3E–H) of control and PEX eyes. A preliminary visual inspection of the stiffness images reveals a conspicuous reduction of YME in both the LC (Figs. 3C, 3D) and ppSC (Figs. 3G, 3H) in PEX specimens compared with control specimens.

For a quantitative analysis, the median of all remaining local YMEs (after excluding irrelevant areas and applying the fit-quality criterion) was calculated for every stiffness image. This way, each force map was represented by a single median YME value (Fig. 4A). As no regional differences in tissue stiffness were observed between central, midperipheral, and peripheral regions of the LC, the three corresponding values were pooled and averaged for subsequent comparative analysis between the groups (Fig. 4B). This procedure yielded a mean YME of 17.2 (±2.7) kPa and 10.1 (±1.4) kPa for the LC of control and PEX eyes, respectively. The corresponding YME values for the ppSC were 158.3 (±59.8) kPa in control and 85.8 (±16.9) kPa in PEX

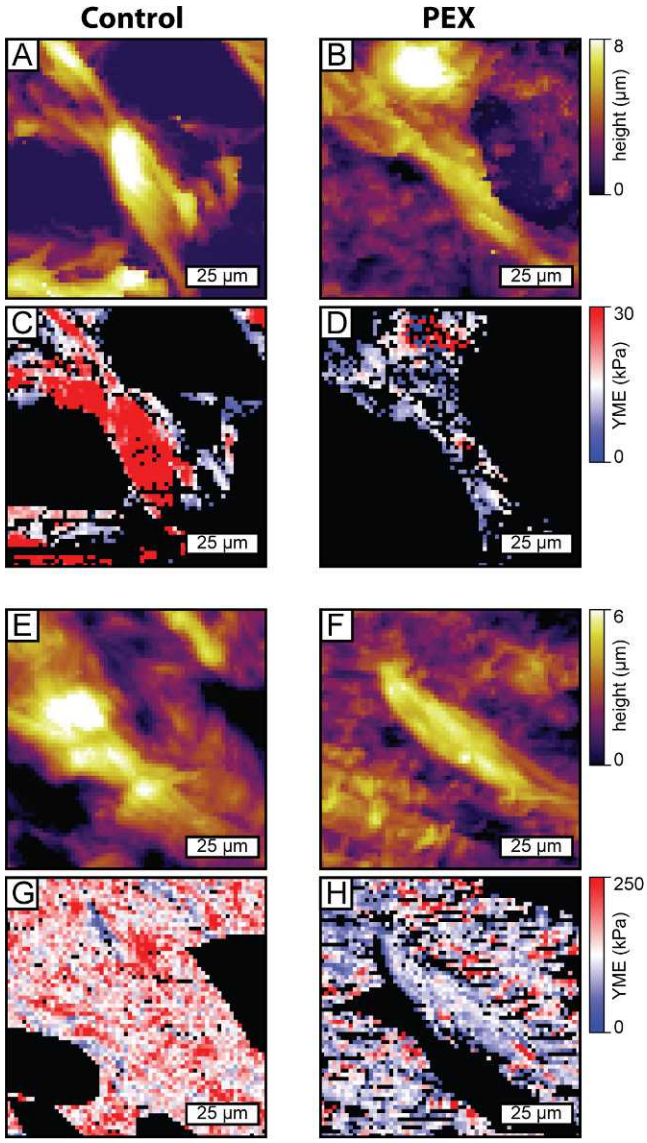

Figure 3. Representative examples of AFM topography and stiffness images obtained from control and PEX specimens. (**A**, **B**) Topography images of representative laminar beams: *left*, control eye; *right*, PEX eye. (**C**, **D**) Corresponding stiffness images. Irrelevant areas and unsatisfactory Hertz fits are masked out (*black*). The PEX-specific decrease in YME is evident from a preponderance of blue over red pixels. (**E**, **F**) Representative topography images of peripapillary sclera: *left*, control eye; *right*, PEX eye. (**G**, **H**) Corresponding stiffness images. Irrelevant areas and unsatisfactory Hertz fits are masked out (*black*). The PEX-specific decrease in peripapillary sclera tissue stiffness is again evident.

samples. In both PEX and control specimens, the YME values were significantly higher (about 9-fold) in the ppSC than in the LC ($P < 0.01$, unpaired Student's *t*-test). In addition, the data revealed a PEX-specific decrease in YME by 41% in the LC and by 46% in the ppSC, which was statistically significant for the LC despite the small sample size ($P < 0.01$, unpaired Student's *t*-test). A detailed overview of the median YME values derived from all measurements taken is given in Table.

Discussion

A growing body of evidence suggests that IOP-related stress and strain affecting the load-bearing connective tissues of the

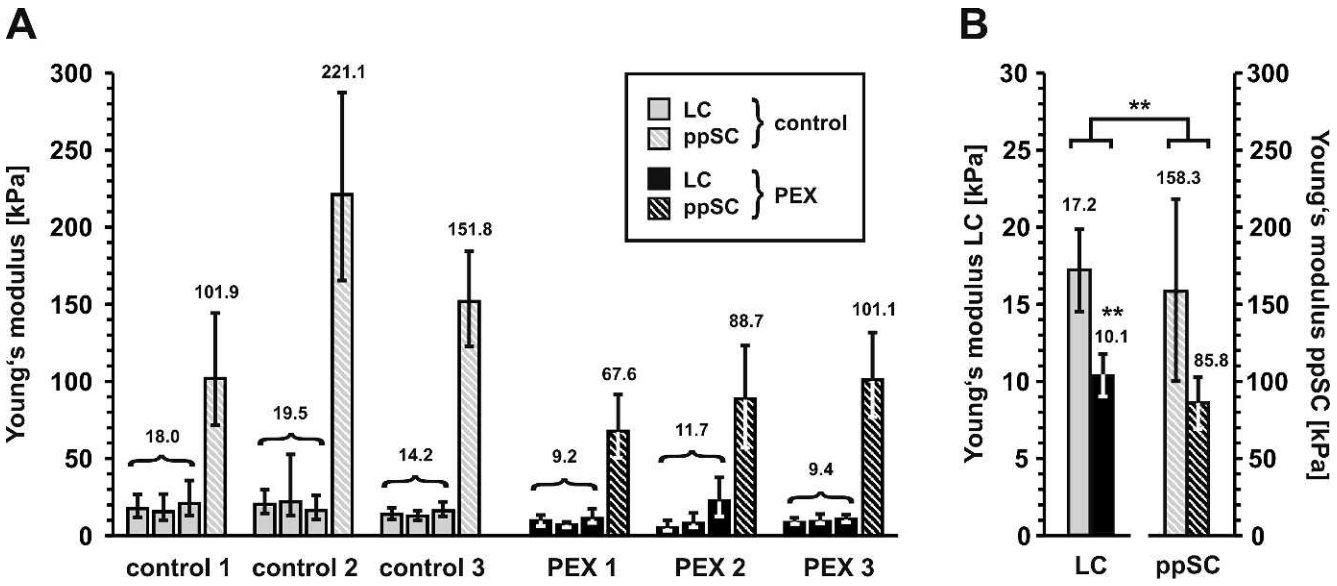

Figure 4. Quantitative analysis of LC and ppSC stiffness in control and PEX eyes. (**A**) Median stiffness per force map. Median stiffness values obtained for the LC and ppSC from every stiffness image taken in all specimens. Error bars depict the interquartile ranges. (**B**) Mean median YME values of LC and ppSC calculated per group. Error bars show the standard deviation. The ppSC displays a 9-fold higher stiffness compared with the LC in both the control and PEX group ($P < 0.01$, unpaired Student's *t*-test). PEX specimens reveal a decrease in stiffness by approximately 40% in the LC ($P < 0.01$, unpaired Student's *t*-test) and the ppSC (not significant, $P > 0.05$, Student's *t*-test).

LC and ppSC are central determinants in the pathophysiology of glaucoma.[27–29] Both the deformability of the LC and ppSC as well as the stresses and strains occurring within these structures in response to IOP are greatly influenced by the structural stiffness of the laminar and scleral connective tissues.[30] Therefore, the local YME as a measure of tissue stiffness may contribute to and indicate an individual's susceptibility to IOP-induced ONH damage. To date, various experimental approaches have been developed to analyze the biomechanical properties of LC and ONH tissues.[30] A common approach for the determination of YME as a measure of stiffness of ONH tissues has been uni- or biaxial tensile testing of tissue strips.[31–34]

AFM, although still markedly underrepresented in ophthalmologic research,[13] has been used to probe the stiffness of ocular cells and tissues, such as cornea, sclera, trabecular meshwork, and lens, in previous studies.[17,35–37] As opposed to tensile tests, this technology relies on local tissue indentation on the nanometer scale with a minute cantilever tip rather than on stretching of entire specimens and may thus yield YME values of a different quality and on a different scale.

To the best of our knowledge, this study is the first to apply AFM nanoindentation to analyze YME as a measure of stiffness in LC and ppSC tissues in human ONH specimens with and without PEX syndrome. As expected, force-map evaluation proved the ppSC to be significantly (about 9-fold) stiffer than the LC in both PEX and control eyes. This finding is in accordance with a higher density of collagen and elastic fibers in the peripapillary region compared with the LC.[38,39]

Despite the small number of specimens included in this study, force map analysis revealed a pronounced and statistically significant decrease in YME of LC specimens obtained from PEX eyes compared with control eyes. This difference becomes even more impressive in view of the older mean age of the PEX eyes (84.3 years) compared with control eyes (74.6 years), since aging has been reported to be associated with a stiffening of the LC,[40] probably as a result of an increased accumulation of type I, III, and IV collagens[41,42] and elastin[43] in combination with a thickening of the LC.[44] The similarly pronounced reduction in stiffness of ppSC tissue of PEX eyes was statistically not significant, probably due to larger interindividual variations.

Table. Median Young's Moduli Derived from the Force Maps*

Eye	YME (kPa)					Age
	Inner LC	Middle LC	Outer LC	Mean (±SD)	ppSC	
Control 1 (No. 473)	17.6 (−6.0/+9.3)	15.5 (−6.4/+11.6)	20.9 (−8.1/+14.7)	18.0 (±2.7)	101.9 (−30.9/+42.3)	88
Control 2 (No. 468)	20.2 (−6.9/+10.0)	22.0 (−9.6/+30.3)	16.3 (−6.2/+10.0)	19.5 (±2.9)	221.1 (−55.2/+65.7)	72
Control 3 (No. 444)	13.8 (−3.2/+4.7)	12.7 (−2.9/+4.0)	16.0 (−4.0/+5.8)	14.2 (±1.7)	151.8 (−29.1/+32.2)	64
Mean (±SD)	17.2 (±3.2)	16.7 (±4.8)	17.7 (±2.8)	17.2 (±2.7)	158.3 (±59.8)	74 (±12)
PEX 1 (No. 340)	9.7 (−3.5/+3.8)	6.9 (−2.0/+2.3)	11.1 (−3.4/+6.9)	9.2 (±2.1)	67.6 (−17.2/+25.0)	84
PEX 2 (No. 227)	4.9 (−2.0/+5.6)	7.9 (−3.2/+7.6)	22.4 (−10.5/+16.5)	11.7 (±9.4)	88.7 (−32.1/+36.0)	77
PEX 3 (No. 236)	8.4 (−2.3/+3.5)	9.2 (−2.5/+4.4)	10.6 (−2.6/+4.1)	9.4 (±1.1)	101.1 (−24.2/+31.9)	92
Mean (±SD)	7.7 (±2.5)	8.0 (±1.1)	14.7 (±6.7)	10.1 (±1.4)	85.8 (±16.9)	84 (±8)

* Median YME values are provided for each LC and ppSC stiffness image generated in every eye investigated. Interquartile range is given in parentheses. Mean and standard deviation are provided where indicated.

A possible explanation for these PEX-associated decreases in YME may be provided by previous work conducted by some of the authors demonstrating structural alterations of the elastic fiber system, which included a disorganized and fragmented elastic fiber network of the LC in PEX eyes without glaucoma.[11] These elastotic alterations were already present at very early stages of the disease, suggesting a primary disturbance in elastin metabolism, and were associated with a significant downregulation of elastic fiber constituents (elastin, fibrillin-1, fibulin-4) and lysyl oxidase-like 1 (LOXL1). LOXL1 is a member of the enzyme family of lysyl oxidases, which catalyze the cross-linking of elastin and collagen fibers.[45] LOXL1 was shown to be specifically required for formation and maintenance of functional elastic fibers by mediating the cross-linking of soluble tropoelastin to insoluble elastin polymers through induction of covalent desmosine and isodesmosine bonds.[45,46] Common single nucleotide polymorphisms in the LOXL1 gene have been identified as principal genetic risk factors for both PEX syndrome and PEX glaucoma in all geographic populations studied.[47,48] Although the causative functional role of the missense changes caused by the disease-associated variants remains unclear, previous studies have provided evidence for a dysregulated expression of LOXL1 in ocular tissues including the LC of PEX eyes.[11,49,50] Elastotic alterations resulting from LOXL1 deficiency may, therefore, adversely affect the biomechanical properties of the LC and contribute to the decrease in YME demonstrated in this study.

Since YME as a measure of stiffness is among the factors influencing tissue deformation in response to load,[30,51] the marked decline in YME of LC and ppSC connective tissues in PEX eyes may imply an increased deformability of the ONH in response to IOP. By conferring mechanical damage to the optic nerve axons, this may render the ONH more susceptible to IOP-induced damage and constitute a strong risk factor for the development of PEX glaucoma. In fact, eyes with PEX glaucoma display an increased vulnerability to glaucomatous damage compared with eyes with primary open-angle glaucoma (POAG). At a given level of IOP, the probability of exhibiting glaucomatous damage was shown to be higher in eyes with PEX than in those without.[6,52] Moreover, patients with untreated PEX glaucoma progressed considerably faster than those with untreated POAG or normal tension glaucoma.[8] The conclusion from these clinical studies was that the joint effect of IOP elevation and the PEX process itself, which may involve an increased vulnerability of the ONH to IOP-induced damage, confers a greater risk of glaucomatous optic neuropathy in PEX patients compared to those without PEX.[53,54] The findings of the present study appear to confirm these assumptions.

There are a number of obvious limitations to the present study. Apart from the small sample size, we are aware that AFM nanoindentation on isolated tissue sections cannot sufficiently mimic the stress-and-strain situation involved in IOP-induced deformation of the LC and its surrounding tissues in situ. Therefore, the YME values measured do not reflect the real values representative of whole eyes. Furthermore, it is known that different techniques of measuring stiffness give different stiffness values,[55] making a direct comparison of these values difficult. For instance, a short-term YME of 118.97 (±2.62) kPa was measured for the bovine inner sclera using micro-indentation.[55] This value is close to the YME of 158.3 (±59.8) kPa we found by AFM nanoindentation for the normal human peripapillary sclera. On the other hand, uniaxial tensile testing gave an instantaneous YME of 33.9 (±3.43) MPa, approximately 200 times larger, in the case of normal monkey sclera.[31] Moreover, the processing of our ONH specimens, which included freezing, sectioning, thawing, etc., prior to AFM analysis, may have introduced further artificial alterations of inherent tissue properties. The question of stiffness alteration due to freezing has been already addressed with other tissues and techniques.[56–58] Overall, these studies found that mechanical properties between fresh and frozen specimens are not significantly different, suggesting that freezing may have only a minor influence on the mechanical properties of the LC. In any case, the comparative analysis of ONH sections obtained from eyes with and without PEX syndrome, which were identically processed, yielded reproducible results and statistically significant relative differences between both groups in spite of the small sample size.

We therefore believe that the findings of this pilot study provide the first evidence for PEX-specific alterations of biomechanical properties (i.e., structural stiffness) of the ONH, encouraging further large-scale analyses. The marked decrease in stiffness of LC and ppSC tissues in PEX eyes may reflect an inherent tissue weakness rendering these eyes more vulnerable to IOP-induced glaucomatous optic nerve damage. These findings may have direct consequences for the clinical management of PEX patients underlining the need for an exact diagnosis, a strict IOP-reducing therapy, and a close follow-up.

Acknowledgments

The authors thank Elke Meyer for providing expert technical assistance.

References

1. Ritch R, Schlötzer-Schrehardt U. Exfoliation syndrome. *Surv Ophthalmol*. 2001;45:265–315.
2. Schlötzer-Schrehardt U, Naumann GOH. Perspective—ocular and systemic pseudoexfoliation syndrome. *Am J Ophthalmol*. 2006;141:921–937.
3. Schlötzer-Schrehardt U, Naumann GOH. Trabecular meshwork in pseudoexfoliation syndrome with and without open-angle glaucoma—a morphometric, ultrastructural study. *Invest Ophthalmol Vis Sci*. 1995;36:1750–1764.
4. Gottanka J, Flügel-Koch C, Martus P, Johnson DH, Lütjen-Drecoll E. Correlation of pseudoexfoliative material and optic nerve damage in pseudoexfoliation syndrome. *Invest Ophthalmol Vis Sci*. 1997;38:2435–2446.
5. Konstas AGP, Mantziris DA, Stewart WC. Diurnal intraocular pressure in untreated exfoliation and primary open-angle glaucoma. *Arch Ophthalmol*. 1997;115:182–185.
6. Topouzis F, Harris A, Wilson MR, et al. Increased likelihood of glaucoma at the same screening intraocular pressure in subjects with pseudoexfoliation: the Thessaloniki Eye Study. *Am J Ophthalmol*. 2009;148:606–613.
7. Grodum K, Heijl A, Bengtsson B. Risk of glaucoma in ocular hypertension with and without pseudoexfoliation. *Ophthalmology*. 2005;112:386–390.
8. Heijl A, Bengtson B, Hyman L, Leske MC. Natural history of open-angle glaucoma. *Ophthalmology*. 2009;116:2271–2276.
9. Netland PA, Ye H, Streeten BW, Hernandez MR. Elastosis of the lamina cribrosa in pseudoexfoliation syndrome with glaucoma. *Ophthalmology*. 1995;102:878–886.
10. Pena JDO, Netland PA, Vidal I, Dorr DA, Rasky A, Hernandez MR. Elastosis of the lamina cribrosa in glaucomatous optic neuropathy. *Exp Eye Res*. 1998;67:517–524.
11. Schlötzer-Schrehardt U, Hammer CM, Krysta AW, et al. LOXL1 deficiency in the lamina cribrosa as a candidate susceptibility factor for a PEX-specific risk of glaucoma development. *Ophthalmology*. In press.
12. Binnig G, Quate CF, Gerber C. Atomic force microscope. *Phys Rev Lett*. 1986;56:930–933.

13. Last JA, Russell P, Nealey PF, Murphy CJ. The applications of atomic force microscopy to vision science. *Invest Ophthalmol Vis Sci*. 2010;51:6083–6094.
14. Burnham NA, Colton RJ. Measuring the nanomechanical properties and surface forces of materials using an atomic force microscope. *J Vac Sci Technol*. 1989;A7:2906–2913.
15. Radmacher M, Fritz M, Kacher CM, Cleveland JP, Hansma PK. Measuring the viscoelastic properties of human platelets with the atomic force microscope. *Biophys J*. 1996;70:556–567.
16. Jiao Y, Schäffer TE. Accurate height and volume measurements on soft samples with the atomic force microscope. *Langmuir*. 2004;20:10038–10045.
17. Last JA, Liliensiek SJ, Nealey PF, Murphy CJ. Determining the mechanical properties of human corneal basement membranes with atomic force microscopy. *J Struct Biol*. 2009;167:19–24.
18. Hertz H. Über die Berührung fester elastischer Körper. *J Reine Angew Math*. 1882;92:156–171.
19. Radmacher M, Cleveland JP, Fritz M, Hansma HG, Hansma PK. Mapping interaction forces with the atomic force microscope. *Biophys J*. 1994;66:2159–2165.
20. Stark RW, Thalhammer S, Wienberg J, Heckl WM. The AFM as a tool for chromosomal dissection—the influence of physical parameters. *Appl Phys A*. 1998;66:579–584.
21. Grant CA, Brockwell DJ, Radford SE, Thomson NH. Tuning the elastic modulus of hydrated collagen fibrils. *Biophys J*. 2009;97:2985–2992.
22. Hutter JL, Bechhoefer J. Calibration of atomic force microscope tips. *Rev Sci Instrum*. 1993;64:1868–1873.
23. Cook SM, Schäffer TE, Chynoweth KM, Wigton M, Simmonds RW, Lang KM. Practical implementation of dynamic methods for measuring atomic force microscope cantilever spring constants. *Nanotechnology*. 2006;17:2135–2145.
24. Schäffer TE. Calculation of thermal noise in an atomic force microscope with a finite optical spot size. *Nanotechnology*. 2005;16:664–670.
25. Gibson CT, Johnson DJ, Anderson C, Abell C, Rayment T. Method to determine the spring constant of atomic force microscope cantilevers. *Rev Sci Instrum*. 2004;75:565–567.
26. Proksch R, Schäffer TE, Cleveland JP, Callahan RC, Viani MB. Finite optical spot size and position corrections in thermal spring constant calibration. *Nanotechnology*. 2004;15:1344–1350.
27. Burgoyne CF, Downs JC, Belezza AJ, Suh JKF, Hart RT. The optic nerve head as a biomechanical structure: a new paradigm for understanding the role of IOP-related stress and strain in the pathophysiology of glaucomatous optic nerve head damage. *Prog Retin Eye Res*. 2005;24:39–73.
28. Downs JC, Roberts MD, Burgoyne CF. The mechanical environment of the optic nerve head in glaucoma. *Optom Vis Sci*. 2008;85:425–435.
29. Downs JC, Roberts MD, Sigal IA. Glaucomatous cupping of the lamina cribrosa: a review of the evidence for active progressive remodelling as a mechanism [published online ahead of print Month day, 2010]. *Exp Eye Res*.
30. Sigal IA, Ethier CR. Biomechanics of the optic nerve head. *Exp Eye Res*. 2009;88:799–807.
31. Downs JC, Suh JKF, Thomas KA, Bellezza AJ, Hart RT, Burgoyne CF. Viscoelastic material properties of the peripapillary sclera in normal and early-glaucoma monkey eyes. *Invest Ophthalmol Vis Sci*. 2005;46:540–546.
32. Downs JC, Suh JKF, Thomas KA, Bellezza AJ, Burgoyne CF, Hart RT. Viscoelastic characterization of peripapillary sclera: material properties by quadrant in rabbit and monkey eyes. *J Biomech Eng*. 2003;125:124–131.
33. Spoerl E, Boehm AG, Pillunat LE. The influence of various substances on the biomechanical behavior of lamina cribrosa and peripapillary sclera. *Invest Ophthalmol Vis Sci*. 2005;46:1286–1290.
34. Eilaghi A, Flanagan JG, Tertinegg I, Simmons CA, Brodland GW, Ethier CR. Biaxial mechanical testing of human sclera. *J Biomech*. 2010;43:1696–1701.
35. Ziebarth NM, Wojcikiewicz EP, Manns F, Moy VT, Parel JM. Atomic force microscopy measurements of lens elasticity in monkey eyes. *Mol Vis*. 2007;13:504–510.
36. Last JA, Pan T, Ding Y, et al. Elastic modulus determination of normal and glaucomatous human trabecular meshwork [published online ahead of print January 10, 2011]. *Invest Ophthalmol Vis Sci*. 2011;52:2147–2152.
37. Grant CA, Thomson NH, Savage MD, Woon HW, Greig D. Surface characterisation and biomechanical analysis of the sclera by atomic force microscopy. *J Mech Behav Biomed Mater*. 2011;4:535–540.
38. Hernandez MR, Luo XX, Igoe F, Neufeld AH. Extracellular matrix of the human lamina cribrosa. *Am J Ophthalmol*. 1987;104:567–576.
39. Quigley HA, Brown A, Dorman-Pease ME. Alterations in elastin of the optic nerve head in human and experimental glaucoma. *Br J Ophthalmol*. 1991;75:552–557.
40. Albon J, Purslow PP, Karwatowski WSS, Easty DL. Age related compliance of the lamina cribrosa in human eyes. *Br J Ophthalmol*. 2000;84:318–323.
41. Hernandez MR, Luo XX, Andrzejewska W, Neufeld AH. Age-related changes in the extracellular matrix of the human optic nerve head. *Am J Ophthalmol*. 1989;107:476–484.
42. Albon J, Karwatowski WSS, Avery N, Easty DL, Duance VC. Changes in the collagenous matrix of the aging human lamina cribrosa. *Br J Ophthalmol*. 1995;79:368–375.
43. Albon J, Karwatowski WSS, Easty DL, Sims TJ, Duance VC. Age related changes in the non-collagenous components of the extracellular matrix of the human lamina cribrosa. *Br J Ophthalmol*. 2000;84:311–317.
44. Kotecha A, Izadi S, Jeffery G. Age-related changes in the thickness of the human lamina cribrosa. *Br J Ophthalmol*. 2006;90:1531–1534.
45. Csiszar K. Lysyl oxidases: a novel multifunctional amine oxidase family. *Prog Nucleic Acid Res Mol Biol*. 2001;70:1–32.
46. Liu X, Zhao Y, Gao J, et al. Elastic fiber homeostasis requires lysyl oxidase-like 1 protein. *Nat Genet*. 2004;36:178–182.
47. Thorleifsson G, Magnusson KP, Sulem P, et al. Common sequence variants in the LOXL1 gene confer susceptibility to exfoliation glaucoma. *Science*. 2007;317:1397–1400.
48. Chen H, Chen LJ, Zhang M, et al. Ethnicity-based subgroup meta-analysis of the association of LOXL1 polymorphisms with glaucoma. *Mol Vis*. 2010;16:167–177.
49. Schlötzer-Schrehardt U, Pasutto F, Sommer P, et al. Genotype-correlated expression of lysyl oxidase-like 1 in ocular tissues of patients with pseudoexfoliation syndrome/glaucoma and normal patients. *Am J Pathol*. 2008;173:1724–1735.
50. Schlötzer-Schrehardt U. Molecular pathology of pseudoexfoliation syndrome/glaucoma—new insights from LOXL1 gene associations. *Exp Eye Res*. 2009;88:776–785.
51. Fung YC. *Biomechanics: Mechanical Properties of Living Tissues*. 2nd ed. New York: Springer; 1993.
52. Davanger M, Ringvold A, Blika S. Pseudo-exfoliation, IOP and glaucoma. *Acta Ophthalmol*. 1991;69:569–573.
53. Puska P, Harju M. Optic nerve head topography in non-glaucomatous, normotensive patients with unilateral exfoliation syndrome. *Graefes Arch Clin Exp Ophthalmol*. 2009;247:1111–1117.
54. Teus MA, Castejon MA, Calvo MA, Perez-Salaices P, Marcos A. Intraocular pressure as a risk factor for visual field loss in pseudoexfoliative and in primary open angle glaucoma. *Ophthalmology*. 1998;105:2225–2230.

55. Yoo L, Reed J, Shin A, et al. Characterization of ocular tissues using microindentation and Hertzian viscoelastic models. *Invest Ophthalmol Vis Sci*. 2011;52:3475–3482.

56. Han B, Bischof JC. Engineering challenges in tissue preservation. *Cell Preserv Technol*. 2004;2:91–112.

57. Weeber HA, Eckert G, Soergel F, Meyer CH, Pechhold W, van der Heijde RGL. Dynamic mechanical properties of human lenses. *Exp Eye Res*. 2005;80:425–434.

58. Stemper BD, Yoganandan N, Stineman MR, Gennarelli TA, Baisden JL, Pintar FA. Mechanics of fresh, refrigerated, and frozen arterial tissue. *J Surg Res*. 2007;139:236–242.